Nanoscale

ROYAL SOCIETY OF CHEMISTRY

COMMUNICATION

View Article Online
View Journal | View Issue

Cite this: *Nanoscale*, 2023, **15**, 19475

Received 13th October 2023,
Accepted 22nd November 2023

DOI: 10.1039/d3nr05170f

rsc.li/nanoscale

Chiral metal–organic cages decorated with binaphthalene moieties†

Cheng Huang,‡[a,b] Jiajia Li,‡[a,c] Xinyuan Zhu [a] and Youfu Wang *[a]

The construction of chiral nanoobjects with atomically precise nanostructures has attracted much more attention in the past decades. However, this field is still in its early stages. We designed and synthesized a series of chiral ligands containing the binaphthalene moiety and isophthalate module. Then, four chiral metal–organic cages (MOCs) were obtained through the coordination between isophthalate modules and copper ions. These chiral MOCs exhibit discrete, uniform and stable structures, good solubility and photoluminescence behaviors.

[a]*School of Chemistry and Chemical Engineering, Frontiers Science Center for Transformative Molecules, Shanghai Jiao Tong University, Shanghai 200240, China. E-mail: wyfown@sjtu.edu.cn*
[b]*Guangxi Key Laboratory of Petrochemical Resource Processing and Process Intensification Technology and School of Chemistry and Chemical Engineering, Guangxi University, Nanning 530004, China*
[c]*School of Materials Engineering, Shanghai University of Engineering Science, Shanghai 201620, China*

†Electronic supplementary information (ESI) available. See DOI: https://doi.org/10.1039/d3nr05170f

‡These authors contributed equally to this work.

Youfu Wang

Dr Youfu Wang obtained his BS (2011) and PhD (2016) degrees in Materials Science from the East China University of Science and Technology (ECUST) in China. After a two-year doctoral exchange study at the University of Chicago (2014–2016), Dr Wang was a National Innovative Postdoctoral Researcher (2016–2018) at the Shanghai Jiao Tong University (SJTU) focusing on precisely modified nanoobjects. Since 2018, he has been an Assistant Professor of Chemistry at the SJTU, where he has started his independent work. His current research interests focus on the construction of functional nanocages (metal–organic cages and conjugated organic cages) and their applications in biomedicine and optoelectronics.

Chirality[1] is widespread in nature, not only at the microscopic level, but also at the macroscopic level. With the discovery of the chirality of amino acids and the chiral structure of proteins by Dutch scientist Jacobus Henricus van 't Hoff, researchers have realized that chirality is crucial to the building processes of life. Chiral molecules,[2] widely studied in biology and chemistry, are a class of molecules characterized by non-recombining mirror symmetry due to their own steric structure. Chiral molecules of different configurations manifest different effects. In the field of optics, chiral molecules offer unique advantages. For instance, the direction of polarization of light can be adjusted by utilizing the optical activity of chiral molecules. Chiral molecules also have enormous potential for applications in fields such as medicine,[3,4] catalysis,[1] and photovoltaics.[5] In order to achieve well-defined effects, scientists have always desired to obtain chiral molecules or chiral materials with a single configuration. Chiral nanomaterials with atomically precise structures have attracted much more attention due to their potential as chiral building blocks to construct specifically designed advanced structures with expected properties. These precise chiral nanoobjects will also help in elucidating the evolution process from the chiral molecular level to the chiral macroscopic level.

Among these precise chiral nanoobjects, metal–organic cages (MOCs)[6–9] constructed by coordination between metal clusters or ions and organic ligands have been rising stars. MOCs possess the functionality of organic ligands and the characteristics of metal clusters or ions. MOCs have precise, discrete and customizable nanostructures at the atomic level and independent cavities. The structure and properties of MOCs can be modulated using adjustments in the choice and ratio of metal clusters or ions and organic ligands, which greatly extends the diversity of MOCs. Due to the advantages of

MOCs such as versatility, easy functionality and high stability, they provide new insights and opportunities for solving key problems in fields such as energy, photovoltaics and nanomedicine.[6,10–12]

In recent years, a number of researchers have combined chirality with MOCs, which has largely expanded the properties and applications of MOCs. For example, Prof. Yan Liu and Prof. Yong Cui designed several chiral MOCs with chiral skeletons from chiral ligands.[13–17] Prof. Chengyong Su utilized chiral metallized triphenanthroline ligands coordinated with Pd^{2+} to construct homochiral MOC enantiomers as chiral catalysts.[18–22] Prof. Xiaoping Zhou introduced various functional groups (*e.g.*, the chiral binaphthol (BINOL) moiety, substituted pyrene, *etc.*) into Pd_nL_{2n}-type (n = 2 or 12) MOCs through post-synthesis covalent modification.[23] The BINOL-modified MOCs are chiral; chiral BINOL and non-chiral pyrene co-modified MOCs exhibit circularly polarized luminescence (CPL) properties.[5,24] Incorporating chirality into the construction of MOCs endows these molecular cages with unique potential in the fields of stereochemistry, nanomedicine, catalysis, and photovoltaics. However, this field is still in its early stages.

Based on the advantages of easy functionalization and well-defined structures of MOCs, we hope to develop a new class of chiral MOCs from specifically designed chiral ligands. We have designed and synthesized a series of chiral ligands containing the chiral binaphthalene moiety and isophthalate module; then, a series of chiral MOCs were constructed (R-*R*/*S*-MOC, R = H/Br) through coordination between chiral ligands and copper ions as shown in Scheme 1.

1,1′-Bi-2-naphthol and 6,6′-dibromo-1,1′-bi-2-naphthol of different chirality were selected as chiral sources to construct chiral ligands with the isophthalate module. After nucleophilic substitution reactions and a hydrolysis reaction, four chiral ligands, H-*R*-L, H-*S*-L, Br-*R*-L, and Br-*S*-L, were obtained. The synthetic route and processes are detailed in Scheme S1 and the Experimental section (ESI†). All the synthesized compounds were structurally confirmed by nuclear magnetic resonance (NMR) and mass spectrometry (Fig. S1–S14, ESI†). Because of the flexible alkyl chains, all the chiral ligands have good solubility in common organic solvents (such as THF, DCM, CH_3CN, and DMF). The isophthalate module is easy to form homoleptic cuboctahedral MOCs in an almost quantitative manner through coordination with copper ions to form $Cu_2(COO^-)_4$ paddlewheel nodes. Then, upon coordination of the chiral ligands with copper ions, homoleptic cuboctahedral shaped chiral MOCs (R-*R*/*S*-MOC, R = H or Br) with molecular formula of $Cu_{24}L_{24}$ were expected to form in high yields (ESI†). Similarly, all the chiral R-*R*/*S*-MOCs (R = H or Br) have good solubility in common organic solvents.

From comparison of the ^{1}H-NMR spectra of chiral ligands and related MOCs in $CDCl_3$ (Fig. S15–18, ESI†), the characteristic peaks of these ligands exhibit obvious shifts and widening in MOCs. Due to the signal interference from residual chloroform, we recorded the ^{1}H-NMR spectra of Br-*R*-L and Br-*R*-MOC in 1,1,2,2-tetrachloroethane-d_2 as shown in Fig. 1A. All the peaks of chiral ligands are shifted to the higher field after the coordination with copper ions, and some peaks merge to become broad peaks.[25] The peaks in the aromatic region

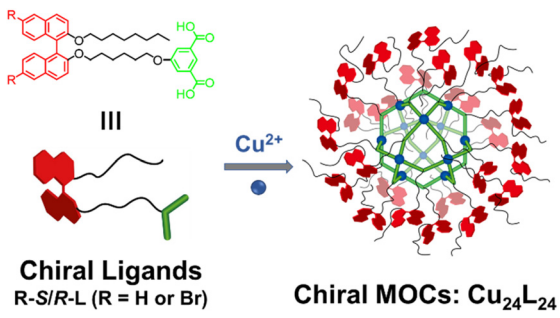

Scheme 1 The construction of chiral MOCs from binaphthalene-based chiral ligands.

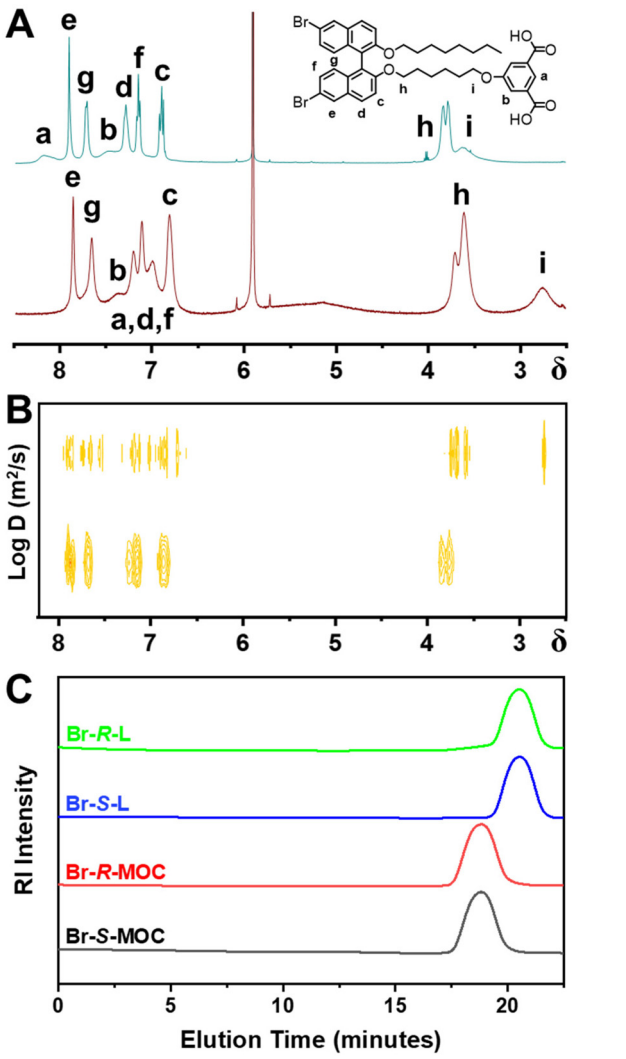

Fig. 1 (A) The ^{1}H-NMR and (B) DOSY spectra of Br-*R*-L and Br-*R*-MOCs. (C) The SEC plots of Br-*R*/*S*-L and Br-*R*/*S*-MOCs.

corresponding to the isophthalate module within Br-*R*-L were at 8.19 and 7.49 ppm, and these shifted to 7.00 and 7.38 ppm, respectively, in Br-*R*-MOC. The characteristic signals from methylene groups linked with 2,2′-binaphthalene moieties (3.81 ppm, dual peaks) and the isophthalate module (3.60 ppm) shifted to 3.61 ppm and 2.74 ppm, respectively. All the aromatic peaks corresponding to the 2,2′-binaphthalene moieties shifted to the higher field and merged into broad peaks. The comparisons of ^{1}H-NMR spectra demonstrated the successful coordination of the chiral ligands with the copper ions.

Two-dimensional diffusion-ordered spectroscopy (DOSY) results, as shown in Fig. 1B, revealed that all the proton resonances of Br-*R*-MOC in 1,1,2,2-tetrachloroethane-d_2 display the same diffusion coefficient,[25,26] proving that the obtained MOC has a discrete and uniform structure. At the same time, the diffusion coefficient of Br-*R*-MOC ($\log D = -10.20$ m^2 s^{-1}) is significantly lower than the diffusion coefficient of Br-*R*-L ($\log D = -9.15$ m^2 s^{-1}) consistent with the much larger hydrodynamic volume of the MOC than that of the ligand. According to the Stokes–Einstein equation, $D = k_BT/6\pi\eta r$ (where D is the diffusion coefficient, k_B is the Boltzmann constant, T is the temperature, η is the viscosity coefficient of solvents, and r is the hydrodynamic radius), the dynamic diameters of the ligand and MOC were calculated to be 0.48 and 4.28 nm, respectively. The hydrodynamic diameters of Br-*R*/*S*-MOC from the dynamic light scattering (DLS) plots are almost the same, at around 4.8 nm and 5.1 nm, respectively, and their respective polydispersity indices (PDIs) are extremely small with values of 0.21 and 0.22 (Fig. S19, ESI†). Considering that the size of the core cuboctahedral MOC is about 3.4 nm, the calculated and measured size of the obtained chiral MOC is reasonable.

Size exclusion chromatography (SEC) was also conducted to measure the molecular weights and the molecular weight distribution (Fig. 1C). Approximately 5 mg of the sample was dissolved in 2 ml of tetrahydrofuran (THF) for SEC.[27] From the SEC plots, both Br-*R*/S-MOCs showed a single sharp peak at around 18.7 min, while both Br-*R*/*S*-L showed a single sharp peak at around 20.5 min. Br-*R*/*S*-MOC had a shorter elution time due to its larger hydrodynamic volume. The molecular weights of Br-*R*/*S*-MOC and Br-*R*/*S*-L calculated from SEC plots were 18 695, 18 708, 820 and 807 g mol^{-1}, respectively, and the PDIs were relatively narrow, with values of 1.04, 1.05, 1.07, and 1.07, respectively. To further clarify the structures of the formed MOCs, we performed matrix-assisted laser desorption ionization time of flight (MALDI-TOF) mass spectrometry. All the measured molecular weights were very close to the theoretical molecular weights (Fig. S20 and Table S1, ESI†), proving the formation of cuboctahedral MOCs with the molecular formula of $Cu_{24}L_{24}$.

The structures of chiral ligands and MOCs were also confirmed using Fourier transform infrared (FT-IR) spectroscopy (Fig. S21, ESI†). Taking Br-*R*/*S*-L and Br-*R*/*S*-MOC as examples, their spectra are quite similar. Both Br-*R*/*S*-L and Br-*R*/*S*-MOC exhibited signals at 3487 cm^{-1}, 1582 cm^{-1}, and 1273 cm^{-1} from the binaphthalene moiety; however, the signal at 1698 cm^{-1} from carboxylic bands within ligands disappeared in the MOCs due to the coordination of Cu^{2+} with the carboxylic acid. From the above results, the obtained MOCs have uniform, discrete and stable nanostructures as expected.

Due to the interesting optical properties of the binaphthalene moiety, we tested the UV-vis absorption and photoluminescence (PL) behaviour of the obtained chiral ligands and MOCs. In THF, the chiral ligands and MOCs showed similar absorbance behaviours and maximum absorbance at 240 nm (Fig. 2A and B, and Fig. S22, ESI†). The PL spectra of the chiral ligands and MOCs in THF excited at 240 nm are quite similar, as shown in Fig. 2A and B (more in Fig. S22, ESI†). The PL signals were detected at around 375 nm, which were slightly widened for the MOCs. Compared with the chiral ligands, the relatively weaker PL intensity of the formed MOCs may be caused by the energy transfer between the closely dense luminescence centers of binaphthalene moieties on the surface of the MOCs. On the other hand, the brominated MOCs exhibited weaker PL intensity in relation to the hydrogen-substituted MOCs caused by the heavy atom effect. Due to the chiral feature of the binaphthalene moiety, the MOCs constructed from ligands decorated with the chiral binaphthalene moiety should exhibit chirality through the chiral transfer. Circular dichroism (CD), a type of rotational spectroscopy used to infer the conformation and configuration of asymmetric structures, was utilized to verify the chiral nature of the ligands and assembled MOCs. 0.1 mg of the samples were dissolved in 2 ml of THF for CD analysis. All the ligands and MOCs in THF exhibited strong CD signals at room temperature (Fig. 2C, D and Fig. S23 in ESI†). Taking Br-*R*-MOC and Br-*S*-MOC as examples, their CD spectra show a good mirror relationship between 200 and 400 nm. This proves that all the obtained MOCs carry chirality from the chiral ligands based on binaphthalene. We also calculated the anisotropic *g*-factor of ligands and MOCs (Fig. S24 and 25, ESI†). The anisotropic

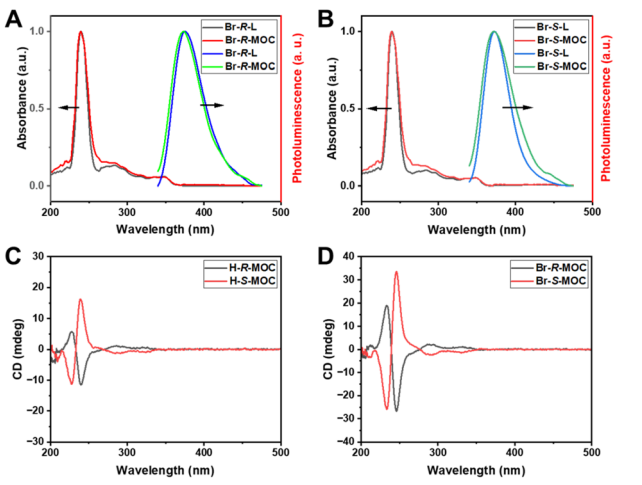

Fig. 2 (A and B) The UV-vis absorbance and photoluminescence spectra of Br-*R*/*S*-L and Br-*R*/*S*-MOCs in THF. (C and D) The CD curves of the obtained chiral MOCs in THF.

g-factors of H-*R*/*S*-MOC were 0.09 and −0.09, and those of Br-*R*/*S*-MOC were −0.28 and −0.29, respectively. These results suggest that chiral brominated MOCs exhibit enhanced anisotropy compared with hydrogen-substituted MOCs.

Because of the chirality and photoluminescence properties of 1,1′-bi-2-naphthol and 6,6′-dibromo-1,1′-bi-2-naphthol, R-*R*/*S*-L and R-*R*/*S*-MOC were expected to exhibit CPL properties. Unfortunately, no obvious CPL signal was found for R-*R*/*S*-L and R-*R*/*S*-MOC in solution or solid form, which might be due to the weak fluorescence of these MOCs.

Due to the heavy atom effect, we expected that Br-*R*/*S*-L and Br-*R*/*S*-MOC should exhibit phosphorescence behaviours. However, in THF, there is no obvious phosphorescence signal even in an inert atmosphere, which might be caused by solvent molecule quenching. Based on this, we performed solid PL tests. This time, both Br-*R*/*S*-L and Br-*R*/*S*-MOC films exhibited phosphorescence signals at around 600 nm excited under 240 nm as shown in Fig. 3A and B. Also, a fluorescence signal at around 420 nm was found. Because of the different states, there is some deviation in the signal between the solution and solid forms. The chiral MOCs based on 6,6′-dibromo-1,1′-binaphthyl ligands exhibit both fluorescence and phosphorescence.

We further tested the phosphorescence lifetime of Br-*R*/*S*-L and Br-*R*/*S*-MOC, and the phosphorescence lifetime of Br-*R*/*S*-L was close to 1 ms, but the phosphorescence lifetime of Br-*R*/*S*-MOC was much reduced (Fig. 3C). This may be due to the presence of dense binaphthalene moieties confined at a similar distance on the MOC surface with ease of contact with each other, which causes energy transfer to induce the decay of the phosphorescence lifetime.

The nitrogen adsorption–desorption isotherms of the chiral MOCs were estimated (Fig. S26, ESI†). A low specific surface area of about 20 $m^2\ g^{-1}$ was found for Br-*R*-MOC, which might be due to the blocking effect from the large number of flexible chains on the surface of the MOCs.

The thermal behaviours of the chiral ligands and MOCs were evaluated using thermogravimetric analysis (TGA). For TGA tests, all the ligands and MOC samples were heated at a rate of 10 °C min^{-1} under a nitrogen flow (Fig. S27, ESI†). All the samples were stable below 400 °C, and then they lost weight quickly in the range of 400–500 °C until they became thermally stable. As shown in Fig. 3D, both Br-*R*-L and Br-*R*-MOC maintained good thermal stability until 400 °C. The slight weight loss of Br-*R*-MOC might result from the volatile solvent molecules combining with copper nodes or loading within the MOC interior. Afterwards, the residues of Br-*R*-MOC not only from the carbonization of ligands, but also from the copper compound quickly decompose. Generally, the obtained chiral MOCs exhibit good thermal stability.

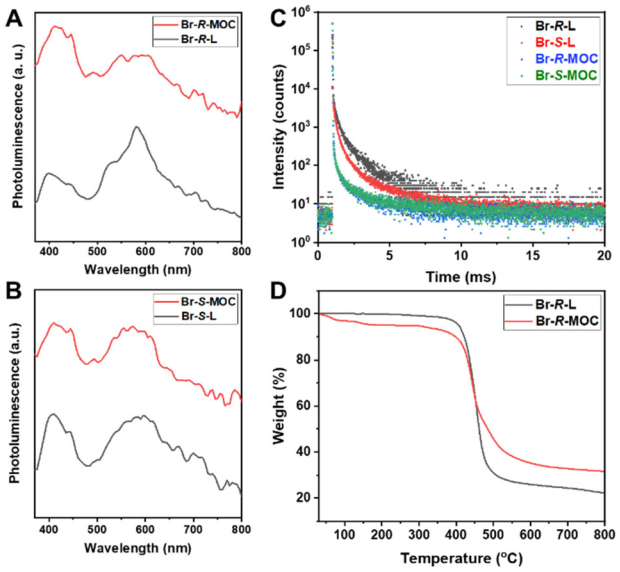

Fig. 3 The phosphorescence spectra (A and B) and lifetime (C) of Br-*R*/*S*-L and Br-*R*/*S*-MOC films (D) the TGA polt of Br-*R*-L and Br-*R*-MOC.

Conclusions

In conclusion, a series of chiral MOCs were constructed through coordination between chiral ligands decorated with binaphthalene moieties and copper ions. The assembled MOCs exhibit uniform, discrete, and stable structures and good solubility in common organic solvents. All the chiral MOCs showed photoluminescence behaviours. The brominated MOCs possess fluorescence and phosphorescence simultaneously in the solid state. The obtained chiral MOCs decorated with binaphthalene moieties enrich the diversity of chiral MOCs and further extend the application of chiral MOCs in optoelectronics. The chiral nanoobjects with atomically precise structures as chiral modules can be further used to assemble complex structures and to deepen the understanding of chiral transfer processes.

Author contributions

C. H. and J. L. contributed equally to this work. Y. W. conceived the idea. C. H. and J. L. conducted most of the experiments. X. Z. supervised the data analysis. C. H. and Y. W. wrote the paper. All authors discussed the results, commented on the paper, and have given approval for the final version of the manuscript.

Conflicts of interest

There are no conflicts to declare.

Acknowledgements

This work was supported by the Fundamental Research Funds for the Central Universities (YG2022QN027 and YG2023QNA04).

References

1 M. Tang and X. Yang, *Eur. J. Org. Chem.*, 2023, **26**, e202300738.
2 M. E. Powell, C. D. Evans, S. D. Bull, T. D. James and P. S. Fordred, in *Comprehensive Chirality*, 2012, pp. 571–599. DOI: **10.1016/b978-0-08-095167-6.00845-4**.
3 W. D. Lubell, K. S. Beauregard and F. Polyak, in *Comprehensive Chirality*, 2012, pp. 86–104, DOI: **10.1016/b978-0-08-095167-6.00104-x**.
4 I. P. Silvestri and P. J. J. Colbon, *ACS Med. Chem. Lett.*, 2021, **12**, 1220–1229.
5 L. Gu, W. Ye, X. Liang, A. Lv, H. Ma, M. Singh, W. Jia, Z. Shen, Y. Guo, Y. Gao, H. Chen, D. Wang, Y. Wu, J. Liu, H. Wang, Y.-X. Zheng, Z. An, W. Huang and Y. Zhao, *J. Am. Chem. Soc.*, 2021, **143**, 18527–18535.
6 A. J. Gosselin, C. A. Rowland and E. D. Bloch, *Chem. Rev.*, 2020, **120**, 8987–9014.
7 J. Liu, Z. Wang, P. Cheng, M. J. Zaworotko, Y. Chen and Z. Zhang, *Nat. Rev. Chem.*, 2022, **6**, 339–356.
8 E. Sánchez-González, M. Y. Tsang, J. Troyano, G. A. Craig and S. Furukawa, *Chem. Soc. Rev.*, 2022, **51**, 4876–4889.
9 D. Zhang, T. K. Ronson, Y.-Q. Zou and J. R. Nitschke, *Nat. Rev. Chem.*, 2021, **5**, 168–182.
10 W. Zhao, Z. He and B. Z. Tang, *Nat. Rev. Mater.*, 2020, **5**, 869–885.
11 A. Zheng, T. Zhao, C. Xiao, X. Jin and P. Duan, *J. Mater. Chem. C*, 2022, **10**, 13084–13092.
12 D. Sun, X. Feng, X. Zhu, Y. Wang and J. Yang, *Coord. Chem. Rev.*, 2024, **500**, 215546.
13 Y. H. Xiao, P. Weidler, S. S. Lin, C. Wöll, Z. G. Gu and J. Zhang, *Adv. Funct. Mater.*, 2022, **32**, 2204289.
14 J. Dong, Y. Liu and Y. Cui, *Acc. Chem. Res.*, 2020, **54**, 194–206.
15 J. Jiao, C. Tan, Z. Li, Y. Liu, X. Han and Y. Cui, *J. Am. Chem. Soc.*, 2018, **140**, 2251–2259.
16 C. Tan, J. Jiao, Z. Li, Y. Liu, X. Han and Y. Cui, *Angew. Chem., Int. Ed.*, 2018, **57**, 2085–2090.
17 X. Tang, H. Jiang, Y. Si, N. Rampal, W. Gong, C. Cheng, X. Kang, D. Fairen-Jimenez, Y. Cui and Y. Liu, *Chem*, 2021, **7**, 2771–2786.
18 K. Wu, K. Li, Y. J. Hou, M. Pan, L. Y. Zhang, L. Chen and C. Y. Su, *Nat. Commun.*, 2016, **7**, 10487.
19 J. Guo, Y. W. Xu, K. Li, L. M. Xiao, S. Chen, K. Wu, X. D. Chen, Y. Z. Fan, J. M. Liu and C. Y. Su, *Angew. Chem., Int. Ed.*, 2017, **56**, 3852–3856.
20 Y. J. Hou, K. Wu, Z. W. Wei, K. Li, Y. L. Lu, C. Y. Zhu, J. S. Wang, M. Pan, J. J. Jiang, G. Q. Li and C. Y. Su, *J. Am. Chem. Soc.*, 2018, **140**, 18183–18191.
21 Y. C. Luo, K. L. Chu, J. Y. Shi, D. J. Wu, X. D. Wang, M. Mayor and C. Y. Su, *J. Am. Chem. Soc.*, 2019, **141**, 13057–13065.
22 J. S. Wang, K. Wu, C. Yin, K. Li, Y. Huang, J. Ruan, X. Feng, P. Hu and C. Y. Su, *Nat. Commun.*, 2020, **11**, 4675.
23 D. Luo, Z. J. Yuan, L. J. Ping, X. W. Zhu, J. Zheng, C. W. Zhou, X. C. Zhou, X. P. Zhou and D. Li, *Angew. Chem., Int. Ed.*, 2023, **62**, e202216977.
24 Z. F. Liu, J. Ren, P. Li, L. Y. Niu, Q. Liao, S. Zhang and Q. Z. Yang, *Angew. Chem., Int. Ed.*, 2022, **62**, e202214211.
25 M. Li, Y. Li, X. Li, F. Wang and Y. F. Han, *Chin. J. Chem.*, 2023, **41**, 1431–1436.
26 Z. Lv, C. Yu, X. Zhu and Y. Wang, *Chemistry*, 2022, **4**, 865–871.
27 C. Yu, P. Yang, X. Zhu and Y. Wang, *Sci. China: Chem.*, 2022, **65**, 858–862.